ADVANCED FUNCTIONAL MATERIALS
www.afm-journal.de

Probe-Based Electro-Oxidative Lithography of OTS SAMs Deposited onto Transparent ITO Substrates

*Daniela Meroni, Silvia Ardizzone, Ulrich S. Schubert, and Stephanie Hoeppener**

Transparent conductive oxides like indium tin oxide (ITO) play a pivotal role in a wide range of innovative applications, such as new generations of solar cells. In many of these applications the tailoring of surface properties on the nanometer scale represents a highly desirable target. The local oxidation of self-assembled monolayers (SAMs) using a scanning probe is a promising technique to achieve surface modifications on the nanometer scale. So far, electro-oxidative lithography of SAMs has been reported mainly on Si wafers while there are no previous reports on transparent oxides. Here, we report the oxidative lithography of *n*-octadecyltrichlorosilane (OTS) SAM deposited onto an ITO layer. A local overoxidation of the substrate is observed while the simultaneously occurring monolayer oxidation is indirectly confirmed by the site-selective deposition of silver nanoparticles onto electro-oxidized areas. The process of lithography is compared to that on OTS-Si substrates and its mechanism is systematically investigated by means of scanning Kelvin probe microscopy (SKPM).

1. Introduction

Transparent conductive oxides are fundamental components in a wide range of technological applications, such as LCDs, flat panel displays, plasma displays, touch panels, electronic ink applications, OLEDs, and solar cells. Among the transparent conductive oxides indium tin oxide (ITO) is currently the most frequently employed because of its high electrical conductivity, good optical transparency, and its ease of film deposition.[1]

The modulation of the surface properties of transparent oxides, such as their wettability, friction, adhesion, and conductivity, is crucial to their integration in highly complex frameworks. To this respect, self-assembled monolayers (SAMs) based on siloxanes have proved reliable and stable systems to tailor the surface properties of oxides and bear technological relevance in several fields, from biotechnology to microelectronics, from sensors to photovoltaics.[2]

Siloxane-modified oxides are successfully employed as active layers and conductive substrates in photovoltaic devices.[2c–e] Indeed, the covalent bond between the siloxane and the oxide enhances the electron transfer within the network and also between the network and the conducting substrate. Moreover, the SAM can improve the compatibility between the oxide and the organic components of solar cells, resulting in a better layer deposition.

Siloxanes may also serve as powerful linkers to attach new functionalities,[3] such as dyes,[4] biomolecules,[5] and nanoparticles,[6] providing a further possibility to tailor the oxide properties. Attaching new functionalities to the oxide surface is even more intriguing if being performed in a controlled fashion. The site-selective oxidation of the SAM by patterning techniques such as microcontact printing, photolithography, or scanning-probe lithography, among others, enables the assembly of complex, hierarchical structures, e.g., by supramolecular chemistry.[7] Among the patterning techniques, the bottom-up approaches, such as electro-oxidative scanning probe lithography and dip-pen lithography,[7] offer a higher resolution than traditional top-down approaches. By combining SAM deposition and electro-oxidative probe lithography, the oxide surface properties can be modified on the nanometer scale.

The literature offers only scanty reports of local oxidation of transparent oxides by techniques such as photolithography,[8] and micro-contact printing,[9] which allow only a much lower resolution than electro-oxidative probe lithography. So far, besides of a study on diamond substrates,[10] electro-oxidative probe lithography has been applied exclusively on Si wafers and no previous reports of its application on transparent oxides are found.

Here, we report for the first time the nanometer scale oxidation of OTS monolayers onto ITO films by electro-oxidative probe lithography. The surface modification induced by oxidation is exploited to achieve a further surface modification by the site-selective growth of Ag nanoparticles. The oxidation process is compared to the oxidation of the bare, non-coated oxide and to OTS-Si, which was chosen as a reference due to its previous application in electro-oxidation lithography studies.[11]

D. Meroni, Prof. S. Ardizzone
Dipartimento di Chimica Fisica ed Elettrochimica
Università degli Studi di Milano
Via Golgi 19, 20133 Milano, Italy
D. Meroni, Prof. U. S. Schubert, Dr. S. Hoeppener
Laboratory of Organic
and Macromolecular Chemistry (IOMC)
Friedrich-Schiller-University Jena
Humboldtstrasse 10, D-07743 Jena, Germany
Jena Center for Soft Matter (JCMS)
Friedrich-Schiller-University Jena
Humboldtstrasse 10, D-07743 Jena, Germany
Abbe School of Photonics
Physikalisch-Astronomische Fakultät
Max-Wien-Platz 1, D 07743 Jena, Germany
E-mail: s.hoeppener@uni-jena.de

DOI: 10.1002/adfm.201200673

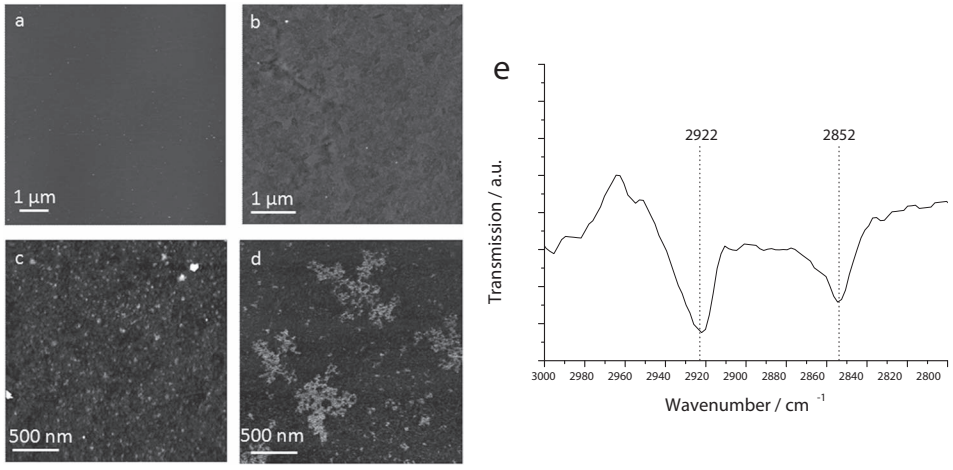

Figure 1. AFM height images recorded in tapping mode of a) OTS-Si and b) OTS-ITO; OTS-ITO samples showing dendritic islands: c) height and d) phase image recorded in tapping mode. e) Granzing angle reflectance mode FT-IR spectrum of an OTS monolayer self-assembled on ITO.

In particular scanning Kelvin probe microscopy (SKPM) is employed in these studies to gain insight into the oxidation mechanism. SKPM is a powerful technique that allows analyzing the variation of the surface potential on the nanometer scale and mapping these changes. So far, this technique has been scarcely exploited in the field of monolayers; only few publications apply it on siloxane-based monolayers deposited on Si systems.[6b,12] In the present study, SKPM is used to investigate the lithographic process in a systematic way and to compare the oxidation mechanism on OTS-coated Si and ITO.

2. OTS Monolayers on ITO

During the monolayer self-assembly, the OTS molecules are hydrolyzed in the presence of water and bind covalently to the oxide surface.[13] Besides the covalent linkage to the substrate, neighboring siloxane molecules give rise to lateral cross-linking, thus, improving the stability of the monolayer.[14]

In this study, an OTS monolayer was deposited on both Si wafers and ITO layers by optimizing the most suitable conditions. The monolayer formation was assessed by water contact angle measurement and the quality of the monolayer was analyzed by AFM investigations. The resulting water contact angles were 105° and 109° for Si and ITO, respectively. The AFM images show a homogeneous coverage of the surface of both the Si wafer and the ITO layer. The latter presents a rougher surface due to the inherent roughness of the ITO layer on float glass substrates (**Figure 1**a,b).

FT-IR measurements performed in the grazing incident reflectance mode additionally confirmed the successful formation of the monolayer. Analysis of the peak positions of the $-CH_2$ stretching vibrations demonstrated a less well arranged monolayer on the ITO monolayer compared to OTS monolayers formed on silicon wafers. Nonetheless, the peaks found at 2922 cm^{-1} and 2852 cm^{-1} are still an indication for a reliably packed self-assembled monolayer on ITO (Figure 1e).

As widely discussed in the literature,[15] the monolayer formation is strongly influenced by the conditions during the deposition, in particular by the atmospheric humidity and water content of the self-assembly solutions. Depending on the humidity conditions and the temperature[3] during the SAM deposition, the obtained monolayers can present dendritic structures observable in AFM phase images recorded in tapping mode (Figure 1d). However, in the current study no effect on the height images was observed (Figure 1c), which occurrence could be interpreted as the formation of an incomplete monolayer. These investigations, in combination with the measured water contact angle of 108°, allows to conclude that a complete OTS monolayer was formed also in these cases. The formation of the dendritic islands is sometimes observed, in particular in tapping mode, also on silicon wafers, where the FT-IR analysis of the $-CH_2$ peaks reveals the formation of a densely packed monolayer.[16] Moreover, the later described electro-oxidation could be performed both on the islands and on the background monolayer. As it will be shown in the next paragraphs, both lithography and site-selective deposition of Ag nanoparticles can be performed onto both the dendritic islands and the rest of the monolayer. Therefore, the dendritic islands might represent regions where the monolayer is more compact, while in the rest of the film the monolayer is still present even if less ordered and compact.

3. Electro-Oxidative Lithography on Silicon Wafers and ITO Substrates

In electro-oxidative lithography, applying a negative bias voltage between a conductive SFM tip and the substrate results in the local oxidation of the surface. The width of the generated patterns depends on the tip dimension and on the patterning conditions, such as the applied voltage, pulse duration and relative humidity.[17] The electro-oxidative lithography of OTS-Si represents a well established technique. The local oxidation causes the conversion of the surface exposed methyl groups of the octadecyl chain into carboxyl functionalities, while for prolonged pulse duration or higher bias, the oxidation of the underlying Si layer can take place, resulting in the growth of SiO_2.[17,18a] The

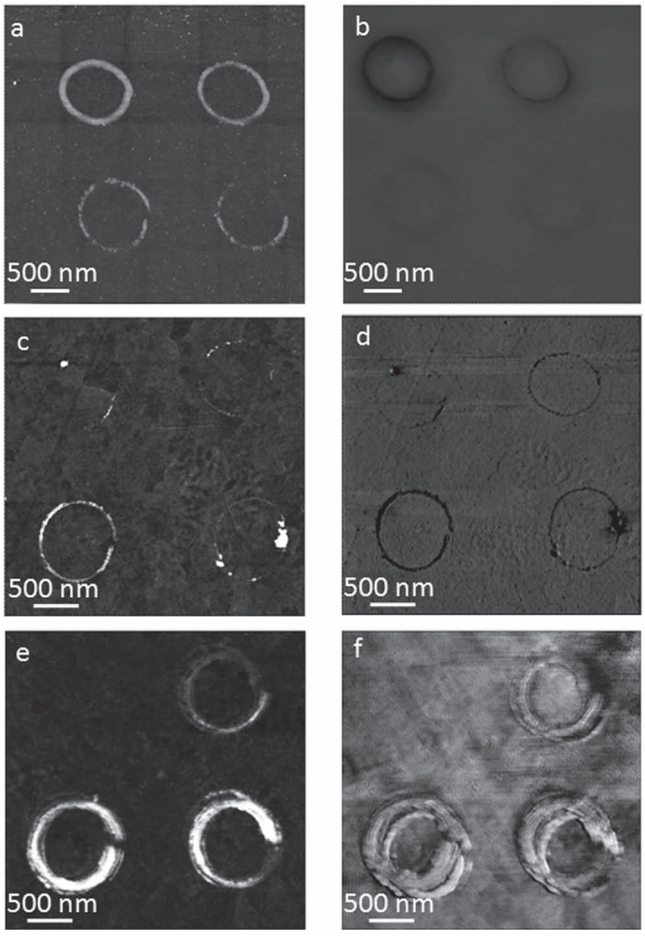

Figure 2. Height images recorded in tapping mode and lateral force images recorded in contact mode for electro-oxidized samples of: a,b) OTS-Si; c,d) OTS-ITO; e,f) ITO.

conversion of $-CH_3$ functions into –COOH groups remarkably alters the properties of the surface; the electro-oxidized regions become hydrophilic, thus showing friction forces much stronger than the unmodified, hydrophobic OTS monolayer. The difference in friction forces can be easily detected in lateral force images recorded in contact mode, whereas the growth of silica causes an increase in height observable in the height images both in contact and tapping mode.[17]

In this work, lithography onto OTS-Si was performed using a bias voltage of –10 V, relative humidity (RH) of 65% and a pulse duration of 3 to 10 ms (**Figure 2**a,b). In the case of OTS-ITO, only incomplete lithography was achieved even by adopting oxidation conditions more severe than those of OTS-Si (bias voltage: –12 V, RH: 75%, pulse duration: 10 to 25 ms). This incomplete lithography may be a result of the disruption of the water meniscus between the AFM tip and the substrate during the oxidation process. In fact, the presence of a stable water meniscus between tip and substrate represents a fundamental requirement in the oxidative lithography.[7b,18a,19] Electrical current decomposes the water present in the meniscus and the decomposition products cause the oxidation of the substrate/monolayer. The disruption of the water meniscus in the case of the OTS-ITO can be caused by a too fast electron exchange between the tip and the surface. The surface resistivity of ITO is in fact higher than the bulk resistivity of silicon; however, the presence of the native oxide layer may play a more crucial role in this respect, which makes the charge injection process less efficient in case of silicon substrates. Such an effect can be effectively avoided by using a Si spacer between the ITO substrate and the electrical circuit (functioning as a resistor in series with the tip/sample resistance), the electron transfer rate can be reduced and complex patterns can be inscribed without the problem of forming non-continous oxidation lines (Figure 2c,d). The same results can be obtained without the Si spacer by using a cantilever with higher resistivity (e.g., phosphorous n-doped Si cantilever (Veeco, force constant: 20 to 80 N/m, resonant frequency: 229 to 287 kHz, resistivity: 1 to 10 Ω cm)).

Lithography onto OTS-ITO in the presence of a Si spacer requires significantly longer pulse duration, higher bias voltage, and humidity compared to OTS-Si. Narrow inscribed lines (<100 nm) can be obtained, whereas the modulation of the line width is more complex compared to lithography performed on OTS-Si. In fact, in OTS-ITO lithography, pulse duration can be varied in a smaller range since increasing the pulse duration over a certain threshold results again in incomplete oxidation patterns, probably caused also here by the disruption of the water meniscus. In any case, the higher roughness of ITO layers with respect of Si wafers decreases the contrast.

In analogy with the oxidative lithography of OTS-Si, an increase in height in the electro-oxidized areas can be observed also for the OTS-ITO. In the case of Si, such an effect is attributed to the growth of SiO_2.[17] In order to understand the origin of the phenomenon in OTS-ITO, electro-oxidative lithography was performed also on bare/non-coated ITO. Using even less severe oxidation conditions (bias voltage: –10 V, RH: 70%, pulse duration: 2 to 7 ms) and inserting a Si spacer, the lithography of bare ITO was achieved (Figure 2e-f). Height images show clearly an increase in height that can tentatively be attributed to overoxidation of the oxide, resulting in crystal growth or phase change.[20]

4. Site-Selective Particle Growth on Chemical Templates

The increase in height observed after lithography of OTS-ITO suggests the occurrence of an overoxidation of the ITO layer. In order to verify if any monolayer oxidation is taking place, i.e., the local conversion of the exposed $-CH_3$ groups of the siloxane chain into –COOH functionalities or other polar functional groups, a site-selective particle growth was tested.

The presence of carboxyl groups in oxidized regions has been previously demonstrated in the case of OTS-Si samples by FT-IR spectroscopy.[18b] Alternatively indirect verification of the presence of such groups is possible by the site-selective synthesis of nanoparticles.[6a,7b] In fact, patterned areas exhibit chemically active surface sites, whereas the non-electro-oxidized areas are chemically inert, thus providing a suitable template structure to guide the site-selective generation of nanoparticles. The process is started by the binding of metal ions onto the carboxyl groups.

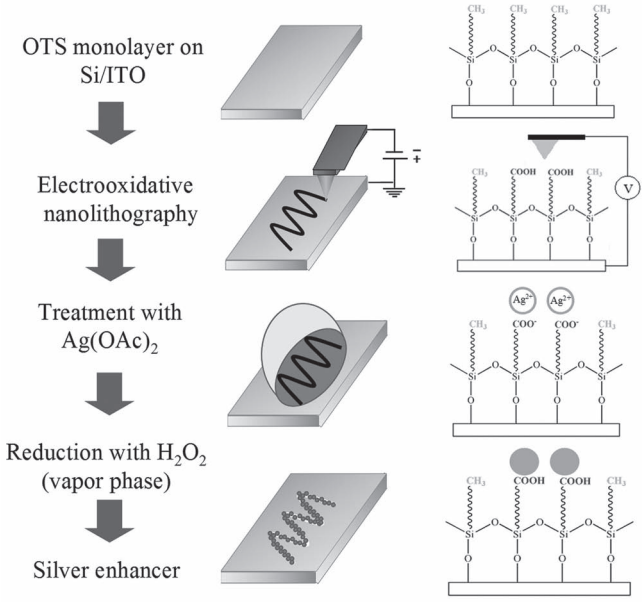

Figure 3. Schematic representation of the process of the selective-growth of Ag nanoparticle on the electro-oxidized areas.

The assembled metal ions are subsequently reduced to generate metal nanoparticles. In this study, Ag nanoparticles were generated by reduction of the metal salts in the gas phase by H_2O_2 (**Figure 3**).

AFM images of the treated OTS-ITO samples show that the oxidized areas are selectively covered (**Figure 4**) with particles, with an apparent particle height of 6 to 7 nm. The presence of the Ag nanoparticles becomes more evident when a silver enhancer process is applied. The growth of the silver particles is the result of an electroless metal deposition process. The Ag nanoparticles exhibit a remarkable stability, as they are stable even against adhesion tape, which was used to clean the substrate from contaminations deriving from the wet-chemical modification procedure. This cleaning process does not affect the non-oxidized surface because of its hydrophobic properties imparted by the OTS monolayer.

Thus, it appears that the formation of polar functional groups, which can be used in subsequent binding reactions, might take place along with the growth of oxide on the ITO substrate in a different way from the case of the overoxidation of an OTS monolayer on silicon.

The selective-growth test was performed also on OTS-ITO samples showing dendritic islands (Figure 4c,d). Electro-oxidized areas on both the dendritic islands and the rest of the monolayer reveal particle coverage, which represents an additional proof for the presence of a complete monolayer on the ITO substrates. Thus it can be proposed that the observed dendritic islands are just more compact and ordered areas of the monolayer.

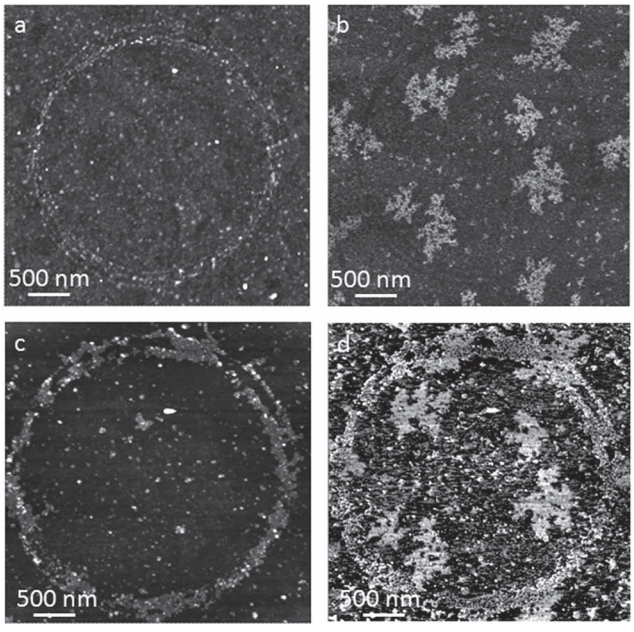

Figure 4. Height and phase images recorded in tapping mode for the electro-oxidized OTS-ITO showing dendritic islands before (a,b) and after (c,d) the site-selctive growth of Ag nanoparticles.

5. Scanning Kelvin Probe Microscopy

All the patterns analyzed using SKPM were electro-oxidized using the same tip and subsequently the surface potential images were acquired using a different tip (the same tip was employed for analyzing all patterns). This procedure allows a more reliable comparison of the SKPM values, as tip geometry and material properties remain comparable. In order to attempt a systematic investigation of the oxidation mechanism, both bare and OTS-coated Si and ITO samples were analyzed. On each substrate, patterns composed of four circles were electro-oxidized by varying the pulse duration, while keeping the bias voltage and the relative humidity constant during each measurement. Measurements were repeated on several patterns for each substrate.

For all samples, SKPM images were recorded using both an AC bias voltage of 1 and 2.5 V, respectively. In the case of the bare substrates, the apparent noise level of the measurements could be significantly improved by lowering the AC bias voltage.

In the case of bare Si (**Figure 5**a,b), only a slight difference in surface potential between electro-oxidized and non-oxidized areas was detected (0 ± 10 mV). This effect can be attributed to the presence of native oxide also on the non-oxidized areas. The presence of native oxide reduces the obtainable contrast with the oxidized structures, which also consists of SiO_x.

Conversely, in OTS-Si samples (Figure 5c,d), the electro-oxidized patterns show a much stronger increase in potential, from +10 to +80 mV, depending on the pulse duration applied during the oxidation process (Figure 5e,f). The average surface potential value of the non-electro-oxidized areas is -10 ± 10 mV (Figure 5e,f). The surface potential measured in the oxidized areas increases with the oxidation time. Saito *et al.*[12a,b] observed a similar increase in surface potential on electro-oxidized OTS-Si samples. The authors attributed the bright

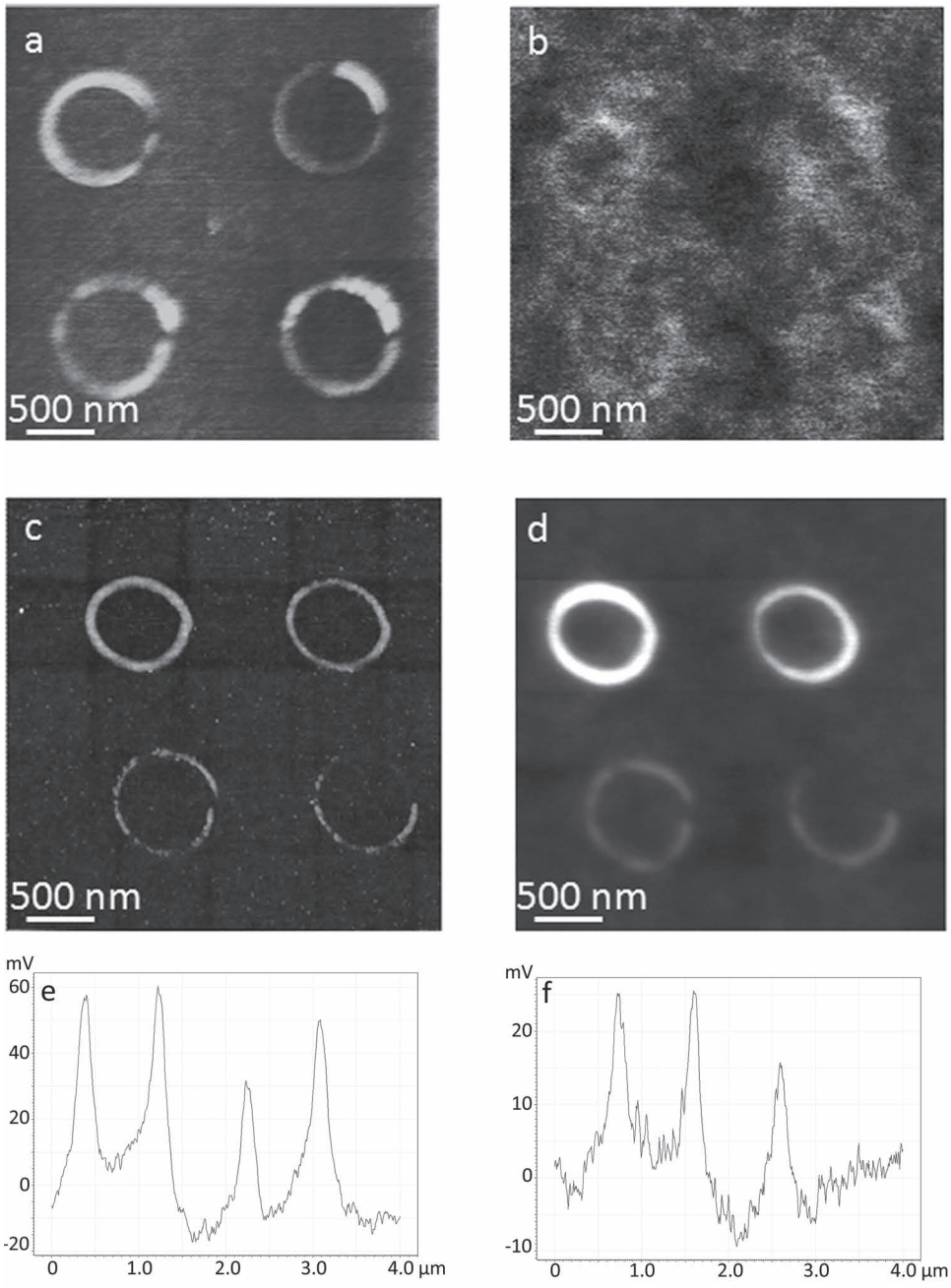

Figure 5. Height images recorded in tapping mode and surface potential images recorded using SPKM for the electro-oxidized samples of: a,b) bare Si and c,d) OTS-Si. Surface potential profiles for the electro-oxidized OTS-Si: e) top circles and f) bottom circles.

areas to non-coated SiO_2, however no other characterization methods were applied to confirm this statement.[14a,b] Furthermore, there is no general consensus in the literature concerning the attribution of the different observed surface potential areas to specific chemical species.[12,a,b,d,e]

Bare ITO (**Figure 6**a,b) shows a completely different behavior: Electro-oxidized areas exhibit a decrease in surface potential and a non-linear relationship between the surface potential and the oxidation time is observed. Moreover, the images show a decreased lateral resolution probably due to the conductivity of the bare ITO layer with respect to the previously investigated samples.

Scanning Kelvin probe microscopy images of electro-oxidized OTS-ITO (Figure 6c,d) are on the other hand very similar to those of OTS-Si. The surface potential average value of non-oxidized areas is –5 ± 8 mV. The observed surface potential increases in the electro-oxidized areas, with values varying from +10 to +60 mV depending on the pulse duration. In analogy with what was observed for OTS-Si, the measured surface potential increases with the oxidation time. The similarity

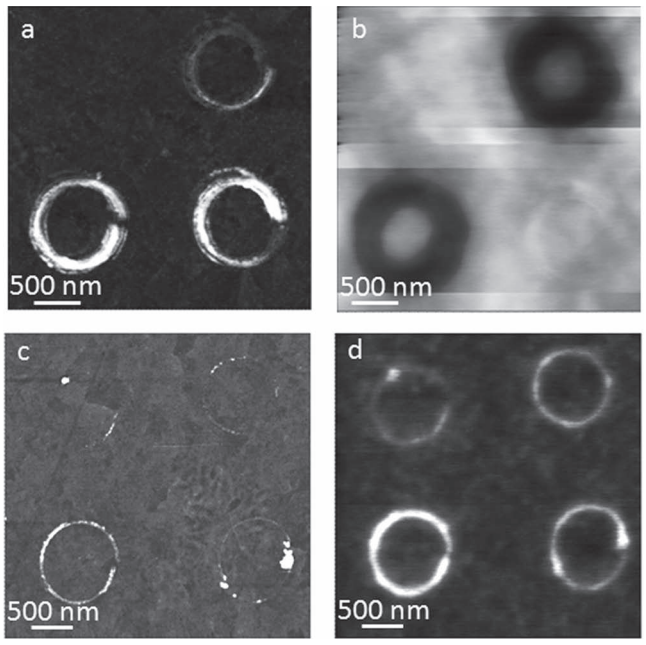

Figure 6. Height images recorded in tapping mode and surface potential images recorded using SPKM for the electro-oxidized samples of: a,b) bare ITO and c,d) OTS-ITO.

between the behavior of OTS-Si and OTS-ITO suggests that OTS effectively shields the substrate surface potential, despite of the distinctive workfunctions and/or electron affinities. These differences in the substrate material become, however, evident in the measurements on the bare substrates. Here no or the opposite oxidation characteristic is observed compared to OTS covered substrates. From these measurements it is evident that the surface potential is mainly influenced by the chemical changes in the electro-oxidized areas and that the contribution of the OTS to the surface potential (e.g., in the non-modified areas) is only minor. Despite of this, the self-assembly of OTS results in a shielding of the inherent substrate's properties and the influence of the substrate can be neglected. This result may be of importance also for the tailoring of the workfunctions of surfaces.

6. Conclusions

The successful electro-oxidative lithography of OTS monolayers deposited onto an ITO film was demonstrated for the first time. The water meniscus between the tip and the substrate plays a pivotal role in the process, even more critical than in the case of OTS-Si substrates. Reducing the rate of electron transfer is fundamental to maintain a stable water meniscus during the oxidation process. This was achieved by either increasing the resistivity of the AFM cantilever or inserting a Si spacer between the ITO layer and the electrical contact. Moreover, particular care has to be placed to adjust the oxidation parameters in order to avoid the disruption of the water meniscus.

The electro-oxidative lithography of OTS-ITO gives rise to two observable effects: A local overoxidation of the substrate takes place, as confirmed by tests onto bare ITO; in addition, the monolayer oxidation causes the conversion of $-CH_3$ groups into hydrophilic functionalities. The latter phenomenon was proven by the site-selective deposition of silver nanoparticles onto electro-oxidized areas.

The process of lithography was additionally studied by means of scanning Kelvin probe microscopy. Surface potential images of OTS-Si and OTS-ITO showed remarkable similarities, while the bare substrates exhibit completely different behavior. Such significant differences, which can be attributed to the presence of the oxidized monolayer, are not observable in the case of topography or lateral force images. Thus, SKPM analysis represents a powerful and unique tool to investigate the mechanism of the monolayer oxidation.

The application of electro-oxidative lithography to substrates other than Si represents a crucial step towards the full exploitation of this technique. Moreover, transparent substrates, such as ITO, represent a family of materials with tremendous applicative interest. The current applications could benefit by the tailoring of critical material properties, such as wettability, adhesion, and conductivity, at the micro/nanometer scale. The presented procedure of electro-oxidative nanolithography of an OTS-ITO layer, coupled with self-assembly of nanoparticles on the electro-oxidized features, bears relevance to numerous fields, from electronics to photovoltaics and sensors. Moreover, the use of electro-oxidized structures as templates for the self-assembly of complex nanostructures is not limited to metal nanoparticles, but can as well be used to guide the self-assembly of polymers or biological molecules, opening the door to innumerable potential applications, as was demonstrated already for electro-oxidized surface templates generated by electro-oxidative lithography on OTS-silicon substrates.[7b]

7. Experimental Section

Materials: *n*-Octadecyltrichlorosilane (Fluka), toluene (Aldrich) and biscyclohexane (BCH, Fluka) were purchased from different suppliers. BCH was distilled over sodium before use. All other reagents were used without further purification. ITO float glass slides (CEC100S) were obtained from PG&O (surface resistivity: 80 Ω/sq). Double side polished p-type silicon wafers (100) were obtained from UniversityWafer (resistivity: 10 to 20 Ω cm). The ITO glass slides and Si wafers were treated for 2 minutes with Ar plasma before use.

Self-Assembly of OTS: OTS monolayers were prepared by immersing the ITO glass slides (or Si wafers respectively) in a solution of OTS (5 µL) in BCH (1 mL) for 1 minute, followed by sonication in toluene. Finally, the slides were dried in a stream of Ar. This procedure was repeated twice. The final water contact angle on ITO samples was 109° (Krüss DSA10). The obtained monolayers were analyzed by atomic force microscopy (AFM, Solver LS AFM, NT-MDT) using Ultrasharp tips (µMash) in tapping mode and by Fourier transform infrared spectroscopy in the grazing angle reflectance mode (FT-IR, Bruker Hyperion spectrometer).

Oxidative Lithography: Electro-oxidative nanolithography was performed using a Ntegra Aura AFM (NT-MDT) placed in a home-built chamber with controllable humidity. Oxidation experiments were carried out at room temperature and at controlled humidity (RH) using a Pt coated AFM tip (µMash). Oxidation patterns were created in "vector mode" (i.e., moving the tip along the trajectories where voltages are to be applied), varying the parameters bias voltage, pulse duration, and relative humidity (RH), while keeping contact force, and temperature constant. Oxidized patterns were imaged afterwards in contact and in tapping mode (using the same tip).

Selective Nanoparticle Growth: Particles were generated by immersing the substrate in an aqueous Ag(II) acetate solution for 10 min, followed by copious rinsing with deionized water and drying in a stream of Ar. The particle formation was initiated by the subsequent reduction of the Ag ions in the vapor phase of hydrogen peroxide for 10 min. The particle coverage could be improved by several cycles of a developing step using a commercial Ag enhancer (Aldrich). Final application of adhesion tape removed contamination and residues from the preparation process, leaving the Ag particles unaffected.

Scanning Kelvin Probe Measurements: The surface potential distribution was characterized by scanning Kelvin probe microscopy (SKPM). The AFM/SKPM instrument (NTegra Aura AFM, NT-MDT) was operated in tapping mode using a Pt coated cantilever (μMasch) with force constant, and resonant frequency values of 1.75 N/m, and 135 kHz (nominal), respectively. A 2.5 V peak-to-peak AC voltage at the resonance frequency of the cantilever was applied between the probe tip and the sample and scanned at frequency of 1.0 Hz. The measurements were performed at ambient humidity (30 to 50% rel. humidity).

Acknowledgements

The work was conducted in the framework of the 'Photonic Nanomaterials' project funded by the German Federal Ministry of Education and Research for excellence in research and innovation. D.M. acknowledges the financial support from Università degli Studi di Milano (PhD school in Chemical Sciences).

Received: March 12, 2012
Revised: May 4, 2012
Published online: June 18, 2012

[1] a) C. G. Granqvist, A. Hultaker, *Thin Solid Films* **2002**, *411*, 1–5; b) D. S. Ginley, J. D. Perkins, in *Handbook of Transparent Conductors*, (Eds: D. S. Ginley, H. Hosono, D. C. Paine), Springer-Verlag, Berlin, Germany **2010**, Ch. 1.

[2] a) W. Senaratne, L. Andruzzi, C. K. Ober, *Biomacromolecules* **2005**, *6*, 2427–2448; b) S. A. Di Benedetto, A. Facchetti, M. A. Ratner, T. J. Marks, *Adv. Mater.* **2009**, *21*, 1407–1433; c) P. Ardalan, T. P. Brennan, H. B. R. Lee, J. R. Bakke, I. K. Ding, M. D. McGehee, S. F. Bent, *ACS Nano* **2011**, *5*, 1495–1504; d) A. J. Morris, G. J. J. Meyer, *J. Phys. Chem. C* **2008**, *112*, 18224–1823; e) C. L. Lin, M. Y. Yeh, C. H. Chen, S. Sudhakar, S. J. Luo, Y. C. Hsu, C. Y. Huang, K. C. Ho, T. Y. Luh, *Chem. Mater.* **2006**, *18*, 4157–4162; f) J. J. Gooding, F. Mearns, W. Yang, J. Liu, *Electroanal.* **2003**, *15*, 81–96.

[3] a) S. Onclin, B. J. Ravoo, D. N. Reinhoudt, *Angew. Chem. Int. Ed.* **2005**, *44*, 6282–6304; b) C. Haensch, S. Hoeppener, U. S. Schubert, *Chem. Soc. Rev.* **2010**, *39*, 2323–2334.

[4] a) X. J. Wang, W. C. Hu, R. Ramasubramaniam, G. H. Bernstein, G. Snider, M. Lieberman, *Langmuir* **2003**, *19*, 9748–9758; b) C. Haensch, S. Hoeppener, U. S. Schubert, *Nanotechnology* **2008**, *19*, 035703–7.

[5] a) Y. Wang, J. Cai, H. Rauscher, R. J. Behm, W. A. Goedel, *Chem. Eur. J.* **2005**, *11*, 3968–3978; b) R. Sfez, L. De-Zhong, I. Turyan, D. Mandler, S. Yitzchaik, *Langmuir* **2001**, *17*, 2556–2559.

[6] a) S. Hoeppener, U. S. Schubert, *Small* **2005**, *1*, 628–632; b) Y. C. Lin, B. Y. Yu, W. C. Lin, Y. Y. Chen, J. J. Shyue, *Chem. Mater.* **2008**, *20*, 6606–6610; c) S. H. Lee, T. Ishizaki, N. Saito, O. Takai, *Appl. Surf. Sci.* **2008**, *254*, 7453–7458; d) M. H. Lin, C.-F. Chen, H.-W. Shiu, C.-H. Chen, S. Gwo, *J. Am. Chem. Soc.* **2009**, *131*, 10984–10991.

[7] a) M. Geissler, Y. N. Xia, *Adv. Mater.* **2004**, *16*, 1249–1269; b) D. Wouters, S. Hoeppener, U. S. Schubert, *Angew. Chem. Int. Ed.* **2009**, *48*, 1732–1739.

[8] a) X. Meng, Y. Lu, B. Yang, G. Yi, J. Jia, *Appl. Mater. Interface* **2010**, *2*, 3467–3472; b) N. Herzer, M. M. Wienk, P. Schmit, A. B. Spoelstra, C. E. Hendriks, S. D. Oosterhout, S. Hoeppener, U. S. Schubert, *J. Mater. Chem.* **2010**, *20*, 6618–6621.

[9] a) N. L. Jeon, P. G. Clem, D. A. Payne, R. G. Nuzzo, *Langmuir* **1996**, *12*, 5350–5355; b) H. Park, S. Go, K. Lee, J. Lee, *Electron. Mater. Lett.* **2008**, *4*, 181–183; c) K. Salaita, Y. Wang, C. A. Mirkin, *Nat. Nanotechnol.* **2007**, *2*, 145–155.

[10] M. Yang, D. Wouters, M. Giesbers, U. S. Schubert, H. Zuilhof, *ACS Nano* **2009**, *3*, 2887–2900.

[11] a) S. Hoeppener, J. H. K. van Schaik, U. S. Schubert, *Adv. Funct. Mater.* **2006**, *16*, 76–82; b) N. Herzer, J. H. K. van Schaik, S. Hoeppener, U. S. Schubert, *Adv. Funct. Mater.* **2010**, *20*, 3252–3259; c) T. Druzhinina, S. Hoeppener, N. Herzer, U. S. Schubert, *J. Mater. Chem.* **2011**, *21*, 8532–8536.

[12] a) H. Sugimura, T. Hanji, K. Hayashi, O. Takai, *Adv. Mater.* **2002**, *14*, 524–526; b) H. Sugimura, K. Hayashi, N. Saito, N. Nakagiri, O. Takai, *Appl. Surf. Sci.* **2002**, *188*, 403–410; c) T. Ichii, T. Fukuma, K. Kobayashi, H. Yamada, K. Matsushige, *Nanotechnology* **2004**, *15*, S30–S33; d) B. G. Bush, F. W. DelRio, J. Opatkiewicz, R. Maboudian, C. Carraro, *J. Phys. Chem. A* **2007**, *111*, 12339–12343; e) S. H. Lee, T. Ishizaki, N. Saito, O. Takai, *Appl. Surf. Sci.* **2008**, *254*, 7453–7458; f) M. H. Lin, C. F. Chen, H. W. Shiu, C. H. Chen, S. Gwo, *J. Am. Chem. Soc.* **2009**, *131*, 10984–10991.

[13] J. Sagiv, *J. Am. Chem. Soc.* **1980**, *102*, 92–98.

[14] a) R. Maoz, H. Cohen, J. Sagiv, *Langmuir* **1998**, *14*, 5988–5993; b) M. D. Rowe-Konopacki, S. G. Boyes, *Macromolecules* **2007**, *40*, 879–888; c) D. Meroni, S. Ardizzone, G. Cappelletti, M. Ceotto, M. Ratti, R. Annunziata, M. Benaglia, L. Raimondi, *J. Phys. Chem. C* **2011**, *115*, 18649–18658.

[15] a) A. V. Krasnoslobodtsev, S. N. Smirnov, *Langmuir* **2002**, *18*, 3181–3184; b) B. G. Bush, F. W. DelRio, J. Opatkiewicz, R. Maboudian, C. Carraro, *J. Phys. Chem. A* **2007**, *111*, 12339–12343.

[16] R. Maoz, J. Sagiv, D. Degenhardt, H. Möhwald, P. Quint, *Supramol. Sci.* **1995**, *2*, 9–24.

[17] D. Wouters, R. Willems, S. Hoeppener, C. F. J. Flipse, U. S. Schubert *Adv. Funct. Mater.* **2005**, *15*, 938–944.

[18] a) R. Maoz, S. R. Cohen, J. Sagiv, *Adv. Mater.* **1999**, *11*, 55–61; b) R. Maoz, E. Frydman, S. R. Cohen, S. Sagiv, *Adv. Mater.* **2000**, *12*, 424–429.

[19] a) H. Sugimura, N. Nakagiri, *Jpn. J. Appl. Phys.* **1995**, *34*, 3406–3411; b) S. Hoeppener, R. Maoz, J. Sagiv, *Nano Lett.* **2006**, *6*, 1334–1338.

[20] a) K.-S. Park, Y.-J. Choi, J.-G. Kang, Y.-M. Sung, J.-G. Park, *Nanotechnology* **2011**, *22*, 285712; b) G. Folcher, H. Cachet, M. Froment, J. Bruneaux, *Thin Solid Films* **1997**, *301*, 242–248.